Earth and Planetary Science Letters 277 (2009) 365–372

Contents lists available at ScienceDirect

Earth and Planetary Science Letters

journal homepage: www.elsevier.com/locate/epsl

On the stability of landslides: A thermo-poro-elastic approach

Liran Goren [a,*], Einat Aharonov [b]

[a] Department of Environmental Sciences and Energy Research, Weizmann Institute of Science, Rehovot 76100, Israel
[b] Institute of Earth Sciences, Hebrew University, Givat Ram, Jerusalem 91904, Israel

ARTICLE INFO

Article history:
Received 31 January 2008
Received in revised form 26 October 2008
Accepted 1 November 2008
Available online 17 December 2008

Editor: C.P. Jaupart

Keywords:
landslide
thermo-poro-elastic
pore pressure
frictional heating
arrested landslides
catastrophic landslides

ABSTRACT

Motion of a large rock mass down a slope can either take the form of a catastrophic landslide, or can exhibit self-stabilization, where the mass arrests on the slope, after moving only a short distance. In order to study the parameters that control the stability of the sliding process, a thermo-poro-elastic model is investigated both numerically and analytically. This model assumes that the physics controlling sliding stability is dominated by coupling between frictional heating, thermal pressurization and sliding velocity: A temperature increase due to frictional heating causes thermal pressurization within a fluid-saturated shear zone. The pressure rise leads to reduction of frictional resistance, which in turns leads to higher sliding velocities. Results demonstrate that the permeability of the sliding mass is an important factor in controlling the sliding stability: Low permeabilities lead to catastrophic landslides, by allowing high pore pressure to develop and friction to be reduced. In contrast, high permeabilities lead to rapid arrest by promoting pore pressure diffusion. A pore pressure – velocity phase plane is described, divided by a separatrix distinguishing between catastrophic and arrested sliding. In this phase plane minute changes in permeability dictate a bifurcation in the dynamics of landslides. A sensitivity study reveals that various geometrical and mechanical parameters can control the sliding process dynamics in a similar manner. It is hypothesized that a third sliding regime observed in nature, creep sliding, may be generated by a sequence of arrested events, where the number of arrested events/unit time dictates the apparent creep velocity.

1. Introduction

Landslides occur in a variety of geological and geomorphological settings including mountain ranges, stand-alone mountains, volcanic islands, submarine continental slopes and even gentle subaerial slopes. Commonly, large-scale landslides (with failure volumes larger than $10^5 m^3$ (Sidle and Ochiai, 2006)) are characterized by very high sliding velocities of 10–100 m/s (for review of large landslides with exceptional rates of motion and abrupt initiation see Hewitt et al. (2008)). Two examples are the notorious 1963 Vaiont landslide and the 1987 Val Pola landslide both in the Italian Alps. The Vaiont landslide was triggered by ground water level rising caused by artificial damming of a valley. Acceleration of the Vaiont landslide was preceded by years of creeping, correlated to the water level in the reservoir (Helmstetter et al., 2004). Then, in October 1963 a rock mass of 2.5×10^8 m^3 slid into the valley, with a velocity of 20–30 m/s, causing the death of 2500 people downstream as the landslide impact generated a huge wave that overtopped the dam and flooded the valley (Genevois and Ghirotti, 2005). Val Pola landslide was triggered by anomalously high precipitation and rapid glacier melting. It accelerated to velocity of tens to a hundred m/s, and impacted a debris-dam lake at the valley floor, causing a wave of muddy water that claimed 27 lives (Crosta et al., 2004). The Vaiont landslide halted only upon reaching a topographical barrier of a valley floor, while the Val Pola landslide changed its course of traveling when reaching the opposing slope of the valley.

In contrast to such catastrophic events, there are instances in which large slope failures are arrested. These can also be regarded as landslides as they are downward movement of slope forming material composed of natural rocks and soils (Sidle and Ochiai, 2006), but their potential to develop high velocities and large travel distances does not come into play for reasons discussed below. Such an arrested sliding motion is suggested to have occurred as a result of the 1949 eruption of Cumbre Vieja volcano at the Island of La Palma. Day et al. (1999) suggest that a normal fault that appeared along the crest of Cumbre Vieja right after this eruption is connected at its base to a shallow detachment fault, subparallel to the surface. The 4 km wide scar with its maximal 4 m offset (Ward and Day, 2001) is likely a surface expression of an arrested sliding motion along the detachment surface. Gabet and Mudd (2006) describe similar arrested sliding motion as slumps, whose center of mass traveled 1–2 m and their deposits did not evacuate the meters long scars. Similarly, Bartelt et al. (2007) refer to such events as 'starving avalanches' and describe them as small debris avalanches that did not run out onto the valley bottom, but stopped close to where they began.

These observations suggest that gravitational mass movements down slopes may either develop into catastrophic landslides (like

* Corresponding author.
E-mail addresses: liran.goren@weizmann.ac.il (L. Goren), einatah@cc.huji.ac.il (E. Aharonov).

0012-821X/$ – see front matter © 2008 Elsevier B.V. All rights reserved.
doi:10.1016/j.epsl.2008.11.002

Vaiont and Val Pola) or into a self-arresting motion that halts on the slope over which it was initiated. In some cases, these two distinct kinematic regimes can be found along the same area and triggered by a common mechanism (e.g. Gabet and Mudd, 2006). Therefore, the question that needs to be addressed is: what determines the stability of the sliding process of landslides?

The importance of the stability of the sliding process inspired many studies that tackled the problem from various points of view. The effect of variations of mechanical parameters such as shear stress (Davis et al., 1990), friction law (Helmstetter et al., 2004), and evolving porosity (Iverson et al., 2000; Iverson, 2005) lead, in a poro-elastic perspective, to the emergence of two kinematics regimes: catastrophic sliding and steady state constant velocity sliding. Competing infiltration and seepage of fluid (Iverson, 2000; Pouya et al., 2007) was shown to also affect the kinematics and stability of hydraulically triggered landslides. In all the above models, full arrest of initially accelerating slides was not observed, instead, slides either accelerateor attain a constant velocity. However, models that calculate thickness variations of the sliding mass using mass and momentum conservation along the down-slope axis do observe a regime in which full arrest of slides occurs. Stopping distances and stability in these models were controlled by the competition between gravitational driving forces and resistive forces due to dissipation (Mangeney-Castelnau et al., 2003), hydraulic diffusivity (Savage and Iverson, 2003) or erosion effect due to the presence of an erodible bed lying on the slide path (Mangeney et al., 2007). Our present work proposes that a thermo-poro-elastic (TPE) mechanism may also play an important role in controlling whether slides are arrested or accelerated. In the TPE mechanism stability arises from the competition between gravitational driving forces and frictional resisting forces controlled by pore fluid pressure generation and dissipation. The TPE mechanism may operate independent of the slide triggering mechanism (earthquake, volcanic eruption and rain and snow melt infiltration).

The TPE mechanism couples temperature and pore fluid pressure within a fluid-saturated shear zone to the sliding velocity: Rise of pore pressure due to thermal pressurization, induced by shear heating, reduces the normal effective stress and the frictional resistance to sliding, thus allowing higher sliding velocity and higher rates of temperature and pore pressure generation. Indeed, the recent understanding of the major role that the TPE mechanism plays in controlling the runout of landslides (e.g. Voight and Faust, 1982; Davis et al., 1990; Vardoulakis, 2000, 2002; Goren and Aharonov, 2007) motivated us to investigate here how the TPE mechanism may affect the stability of the sliding process. Although TPE mechanisms are commonly invoked both in the study of landslide motion and in motion along faults (Garagash and Rudnicki, 2003; Rempel and Rice, 2006; Rice, 2006), this paper innovatively predicts that two distinct sliding regimes, depending on the shear zone permeability, emerge from the TPE feedback: (1) unbounded catastrophic sliding and (2) arrested motion. A sequence of many arrested events is hypothesized to generate a creeping motion. For natural landslides, the TPE mechanism is expected to couple in a non-linear fashion to other mechanisms controlling sliding stability (e.g. Mangeney-Castelnau et al., 2003; Savage and Iverson, 2003; Mangeney et al., 2007).

Our stability analysis emphasizes the role of permeability, as it is documented to vary by orders of magnitude between different lithological and structural regions (e.g. Saar and Manga, 2004, Fig. 11), with depth (Manning and Ingebritsen, 1999; Saar and Manga, 2004), and also with sliding distance due to mechanical fragmentation of the sliding mass. The importance of permeability to slide triggering and dynamics has been acknowledged before both in the framework of TPE models and in other theoretical, experimental, numerical works (e.g. Haneberg, 1991; Iverson, 1997; Reid, 1997; Turrini and Visintainer, 1998; Lourenço et al., 2006; Rahardjo et al., 2007). In addition to the role of permeability, our analysis demonstrates that the sliding dynamics, controlled by the TPE mechanism, may also depend on other mechanical and geometrical parameters such as shear zone thickness and thermal pressurization coefficient (as demonstrated in Section 4.1). The novelty of our study lies in the analysis that identifies the source of the link between shear zone permeability, and other parameters, and different dynamic regimes of the sliding process (not of slope stability), using a dynamical system approach.

2. Problem Formulation

A large landslide is modeled as a porous block of thickness D sliding down a tilted plane, with a constant slope, δ. The sliding block is simulated as an intact body and deformation is concentrated along a thin shear zone with thickness d at the base of the slide ($d \ll D$) (Fig. 1). The porous sliding block is assumed fluid saturated so that initially the fluid pressure is hydrostatic. To solve for the temporal and spatial evolution of pore pressure within the sliding block and for the temporal evolution of the sliding velocity, a TPE model is used. The pore pressure equation is one dimensional, with elevation coordinate, z, varying between 0 at the base of the sliding block to D at its surface. A full description of the model is given in Goren and Aharonov (2007), but for completeness it is briefly reviewed here.

The pore fluid pressure, $p(z,t)$, in excess of the initial pressure prior to triggering, p_0, , evolves according to:

$$\dot{p} = \frac{k}{\eta S_\sigma}\frac{\partial^2 p}{\partial z^2} + \Lambda\dot{\theta}, \tag{1}$$

where $\dot{p} \equiv \partial p/\partial t$, is the time derivative. The first term on the righthand side of Eq. (1) describes pore pressure diffusion, with a depth independent diffusion coefficient, $k/\eta S_\sigma$, where k, η and S_σ are permeability (m^2), pore fluid viscosity (Pa s) and the unconstrained specific storage (Pa^{-1}), respectively. The second term describes pore pressure generation by thermal pressurization, where Λ is the thermal pressurization coefficient ($Pa°C^{-1}$) (Voight and Faust, 1982; Vardoulakis, 2000; Rempel and Rice, 2006; Rice, 2006), and θ is the temperature. Eq. (1) encapsulates two assumptions that are adopted here for simplicity. First, the permeability, k, is taken here as time and depth independent. In reality, k is expected to vary with depth and time due to fragmentation of the sliding body. Second, porosity evolution within the shear zone during the initial stages of sliding should add another term to Eq. (1). A dilative shear zone, with pore volume expansion, will act to reduce pore pressure while a contractive shear zone is expected to increase pore pressure (Iverson, 2005). The constant porosity assumption adopted here mimics the case where the sliding block has already evolved to its critical porosity characterizing granular systems under shear (Iverson et al., 2000;

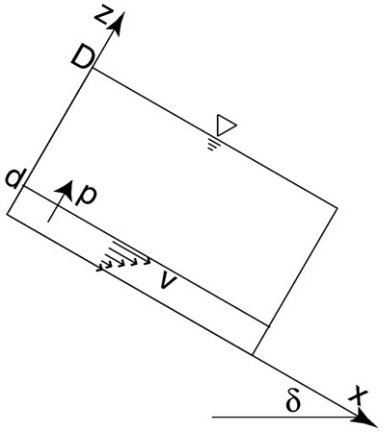

Fig. 1. Model geometry. A porous block slides down a slope tilted δ. The block thickness is D and the shear zone thickness is d. The sliding movement occurs along the x axis and excess pore pressure is diffused along z direction.

Aharonov and Sparks, 2002, and references therein). These simplifications are adopted here in order to clarify the physics of the mechanism, and will be addressed in future versions of the model.

In the model used here, temperature is considered to evolve solely by frictional heating caused by sliding within the shear zone. The temperature relaxation processes of conduction and advection are neglected due to their long time scales (10^4 – 10^6 s), relative to the rapid slide motion, as calculated in Goren and Aharonov (2007). Following this approximation, within the shear zone

$$\rho c\dot{\theta} \simeq \frac{v}{d}\tau(p) \quad \text{for } 0 < z \le d, \tag{2}$$

where $\rho = (1-n)\rho_s + n\rho_f$ and $c = (1-n)c_s + nc_f$ are the density in kg m^{-3} and specific heat in J kg^{-1} °C^{-1} of the solid-fluid mixture (Vardoulakis, 2000). Subscripts s and f stand for the solid and fluid respectively and n is the porosity. $\tau(p) = \mu(\rho g D\cos\delta - p_0 - p)$ is the shear stress where μ is the tangent of the angle of internal friction, and g is gravity in m s^{-2}. v/d is the velocity gradient along the shear zone, assuming a linear velocity profile (Aharonov and Sparks, 2002). Above the shear zone

$$\dot{\theta} \simeq 0 \quad \text{for } d < z \le D. \tag{3}$$

Assigning Eqs. (2) and (3) into (1), and performing a non-dimensional analysis, the pore pressure evolution may be written

$$\dot{\hat{p}} = M\hat{k}\frac{\partial^2\hat{p}}{\partial\hat{z}^2} + R\hat{v}\left(\Sigma - \hat{p}\right) \quad \text{for } 0 < \hat{z} \le N \tag{4}$$

$$\dot{\hat{p}} = M\hat{k}\frac{\partial^2\hat{p}}{\partial\hat{z}^2} \quad \text{for } N < \hat{z} \le 1. \tag{5}$$

The velocity of the sliding mass is derived from force balance considerations for the simplified rigid body slide (Vardoulakis, 2000):

$$\dot{\hat{v}} = N\left[\sin\delta - \mu\left(\Sigma - \hat{p}\right)\right]. \tag{6}$$

where the 'hat' notation implies non-dimensionality. Eqs. (4)–(6) form a complete set of coupled partial differential equations for the pore pressure, $\hat{p}$, and velocity, $\hat{v}$, with non-dimensional variables: $\hat{p} = p/\rho g D$, $\hat{z} = z/D$, $\hat{v} = v/\sqrt{gD}$, $\hat{t} = t\sqrt{gD}/d$ and $\hat{k} = k/k_0$. The non-dimensional parameters controlling the system of Eqs. (4) – (6) are: $M = k_0 d/\eta S_\sigma \sqrt{gD}D^2$, $R = \Lambda\mu/\rho c$, $\Sigma = \cos\delta - \hat{p}_0(\hat{z})$, $N = d/D$ and k_0 is a typical permeability.

3. Numerical Simulations

The system of Eqs. (4) – (6) is solved numerically, using an explicit finite differences scheme. Hydrostatic pore pressure prior to sliding onset is $\hat{p}_0(\hat{z}) = \cos\delta\rho_f(1-\hat{z})/\rho$. The boundary conditions for the non-dimensional pore pressure are taken as impermeable bottom, $\partial\hat{p}/\partial\hat{z}(\hat{z}=0,\hat{t}) = 0$, and drained surface, $\hat{p}(\hat{z}=1,\hat{t}) = 0$. Table 1 presents parameter values used in simulations. We investigate two sets of initial conditions ($\hat{v}_{init}$, $\hat{p}_{init}$), representing different triggering mechanisms: (1) Simulations of type *A*, where $\hat{v}_{init} = 0$ and $\hat{p}_{init} > 0$, correspond to fluid pressurization within the shear zone by either fluid addition due to rain infiltration, mechanical pressurization due to tectonic stresses, or by thermal pressurization by a heat source such as dike emplacement (e.g. Aharonov and Anders, 2006). (2) Simulations of type *B*, where $\hat{p}_{init} = 0$ and $\hat{v}_{init} > 0$, correspond to cases where an external acceleration (e.g. from an earthquake or a volcanic eruption) supplies the block with an initial velocity, while fluid was neither added to the shear zone nor initially pressurized within it.

Fig. 2 shows pore pressure evolution within the shear zone and the sliding velocity of type *A* and *B* simulations, where arrows indicate temporal evolution. All simulation exhibits similar behavior during sliding onset, with velocity increase and PP decrease for type *A* simulations, and velocity decrease and PP increase for type *B* simulations. After some time the behavior bifurcates between two regimes depending on the assigned parameters M, R, and $\hat{k}$. In the following analysis and in Fig. 2 we choose to concentrate on bifurcations that occur due to variations in the permeability, $\hat{k}$. For type *A* simulations (Fig. 2a), bifurcation occurs after ~2.5 s from sliding onset. When $\hat{k} < \hat{k}_c$, where $\hat{k}_c$ is the dimensionless critical permeability separating the two regimes, v and p rise and sliding accelerates. A distinctively different sliding regime is observed when $\hat{k} < \hat{k}_c$: here, after ~2.5 s from the sliding onset, sliding decelerates. For $\hat{k} \gtrapprox \hat{k}_c$, the slide halts after about 14 s having moved 0.4 m and attaining a maximum velocity of ~4.2 cm/s. Type *B* simulations show a similar stability bifurcation (Fig. 2b) that occurs after 5 s. For $\hat{k} < \hat{k}_c$, $\hat{v}$ starts to grow rapidly. For $\hat{k} > \hat{k}_c$, at the bifurcation point, both $\hat{p}$ and $\hat{v}$ decrease until the slide halts after several seconds. The travel distance of an arrested slide with $\hat{k} \gtrapprox \hat{k}_c$ is 0.9 m, and the sliding duration is 21 s.

The loop along the $\hat{k}$=6.9 curve in Fig. 2a (see inset) results from the evolution of pore pressure outside the shear zone by diffusion. Initially, the curve follows the arrested regime behavior, but then, pore pressure outside of the shear zone accumulates to high enough values so that the diffusion rate from the shear zone slows down and the curve loops to continue along a catastrophic regime.

To understand how minute changes (of about a percent) in the permeability may lead to such diverging dynamical behavior, a simplified form of Eqs. (4) – (6) is studied analytically.

Table 1
Variables and parameters used in Sections 2 - 4

Symbol		Value
Variables:		
p (Pa)	Pore pressure	
v (m/s)	Velocity	
θ (°C)	Temperature	
τ (Pa)	Shear stress	
Parameters:		
d	Shear zone thickness	0.1 m
D	Block thickness	100 m
n	Porosity	0.3
ρ_s	Solid density	2700 kg m^{-3}
ρ_f	Fluid density	1000 kg m^{-3}
c_s	Solid specific heat	1000 J kg^{-1} °C^{-1}
c_f	Fluid specific heat	4187 J kg^{-1} °C^{-1}
k_0	Reference permeability	10^{-3} m^2[a]
Λ	Thermal pressurization coefficient	0.3×10^6 Pa °C^{-1}
μ	Tangent to the angle of internal friction	0.5
η	Fluid viscosity	10^{-3} Pa s
S_σ	Unconstrained specific storage	3×10^{-9} Pa^{-1}
δ	Slope angle	15°
l	Diffusion length scale	0.28 m[b]
Derived dimensionless coefficients:		
M	$k_0 d/\eta S\sigma\sqrt{gD}D^2$	1.03×10^{-8}
R	$\Lambda\mu/\rho c$	0.035
Σ	$cos\delta - p_0(z=0)$	0.93
N	d/D	10^{-3}
M'	MD^2/l^2	1.29×10^{-3}
Initial conditions:		
$\hat{p}_{init}$	for type *A* simulations	0.07
$\hat{v}_{init}$	for type *B* simulations	4×10^{-3}

[a] Typical permeability of sandstone.
[b] Corresponding to t_d =2.35 s.

4. Analytic Investigation

For the purpose of studying the dynamics of the system of Eqs. (4) and (6) within the shear zone, the diffusion term in (4) is linearized. The second derivative, $\partial^2\hat{p}/\partial\hat{z}^2$, is approximated as $\hat{p}/$

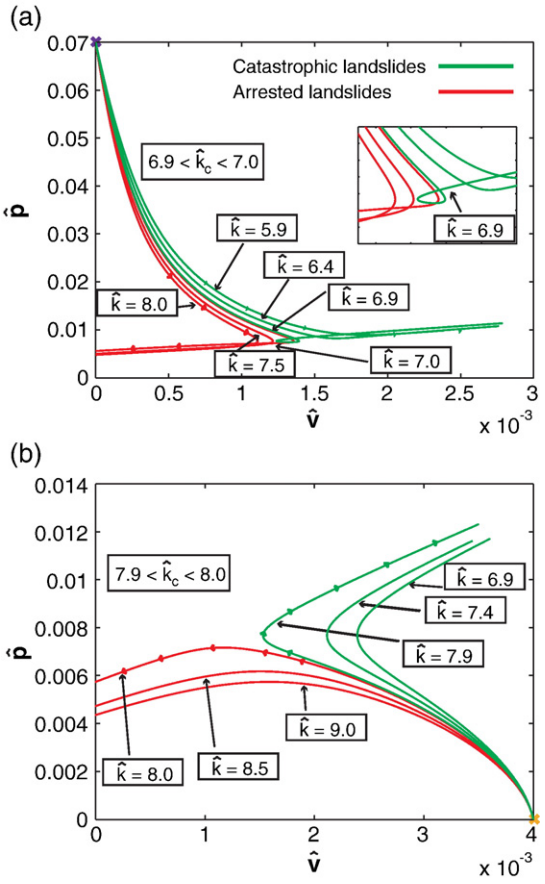

Fig. 2. Numerical simulation results of the evolution of non-dimensional pore pressure along the shear zone, $\hat{p}$, and velocity, $\hat{v}$, for different permeabilities, $\hat{k}$, and parameters from Table 1. For (a) initial condition of type *A* and (b) initial condition of type *B*. $\hat{k}_c$ is the transition permeability between the catastrophic and arrested regimes estimated following the results of the simulations. The loop in the inset of (a) shows that the catastrophic slide with $\hat{k}$=6.9 initially followed an arrested regime, but due to the non-linearity of the diffusion term, accumulation of PP above the shear zone lowered the diffusion rate and caused the slide to evolve as a catastrophic landslide.

(l^2/D^2), where l is a diffusion length scale dictating the distance over which PP is relaxed, and division by D is introduced to obtain a non-dimensional value. Both equations are then a function of time only, and $\hat{p}$ is determined at $\hat{z}=0$. The set of equations to study is then:

$$g(\hat{v},\hat{p}) = \dot{\hat{p}} = -M'\hat{k}\hat{p} + R\hat{v}(\Sigma-\hat{p}) \tag{7}$$

where $M'=MD^2/l^2$, and the velocity equation that remains the same as (6):

$$f(\hat{v},\hat{p}) = \dot{\hat{v}} = N[\sin\delta-\mu(\Sigma-\hat{p})] \tag{8}$$

The system of Eqs. (7) and (8) has only one fixed point at:

$$\begin{aligned} p^* &= \Sigma-\sin\delta/\mu \\ v^* &= M'\hat{k}\mu(\Sigma-\sin\delta/\mu)/R\sin\delta \end{aligned} \tag{9}$$

Here, the location of the fixed point (v^*,p^*) is constrained by physical considerations: $p^*\geq 0$ because in the alternative case when $p^*<0$, the slope is unstable without any additional forcing, a non-natural situation. From Eq. (9), v^* must also be non-negative. To find the nature of the fixed point, the eigenvalues and eigenvectors of the Jacobian matrix, J, are found, where

$$J = \begin{pmatrix} \frac{\partial f}{\partial \hat{v}} & \frac{\partial f}{\partial \hat{p}} \\ \frac{\partial g}{\partial \hat{v}} & \frac{\partial g}{\partial \hat{p}} \end{pmatrix}_{(v^*,p^*)} = \begin{pmatrix} 0 & N\mu \\ \frac{R\sin\delta}{\mu} & \frac{-M'\hat{k}\mu\Sigma}{\sin\delta} \end{pmatrix} \tag{10}$$

(Strogatz, 2000). Since trace(J) < 0 and det(J) < 0, the eigenvalues $\lambda_{1,2}$ are real and have opposite signs, $\lambda_1>0$ and $\lambda_2<0$. Therefore, the fixed point is a saddle point. The slope of the first eigenvector, u_1, is $\lambda_1/N\mu>0$, and the slope of the second eigenvector, u_2, is $\lambda_2/N\mu<0$. In order to evaluate the fixed point (9), and the slope of the eigenvectors, the value of the diffusion length scale, l, must be determined. As such a length scale does not emerge naturally from the model, it can be estimated as $l=\sqrt{k_0 t_d/S_\sigma\eta}$, where $k_0/S_\sigma\eta$ is the characteristic diffusion coefficient and t_d is a time scale related to PP diffusion. Savage and Iverson (2003) for example, find numerically that excess PP is completely dissipated from their modeled slide after 4 s when a relatively large PP diffusion coefficient is used. t_d can be of that order.

Fig. 3 shows the phase plane of system of Eqs. (7) and (8), with the parameters given in Table 1. Fig. 3 demonstrates that the eigenvectors divide the phase plane into four domains. Any initial condition that lies in domains 1 or 2 will eventually lead to an increase of $\hat{p}$ and $\hat{v}$ and catastrophic sliding, while any initial condition that lies in domains 3 or 4 will eventually lead to a decrease of $\hat{p}$ and $\hat{v}$ until the sliding block will reach zero velocity and halt. In short, the eigenvector, u_2, acts as a separatrix distinguishing between two stability

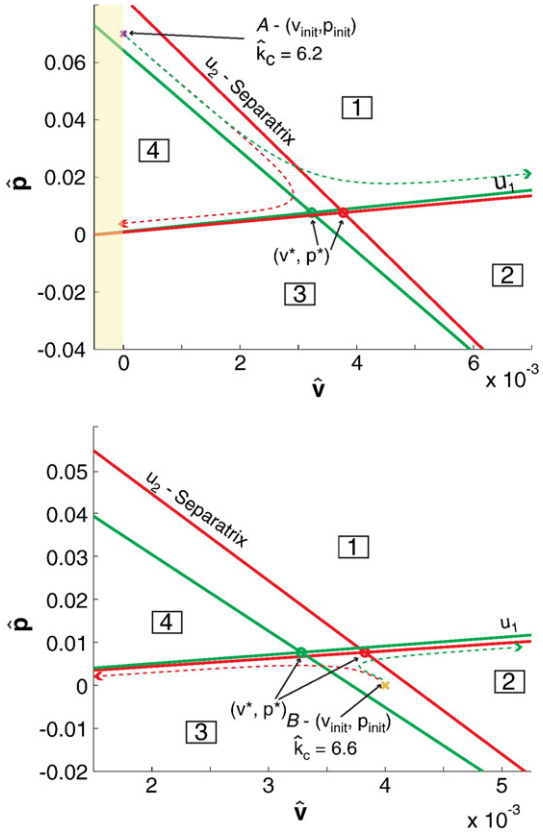

Fig. 3. Phase plane of equation set (7) and (8). Solid lines are the eigenvectors, dashed curves show time evolution, circles are the fixed point and the 'x's represent possible initial conditions of types *A* and *B*. Physical solutions exist only to the right of the shaded area, where $\hat{v}>0$. (a) For initial conditions of type *A* green and red corresponds to permeabilities of $\hat{k}$=5.9 and $\hat{k}$=6.9, respectively. (b) For initial conditions of type *B* green and red corresponds to $\hat{k}$=6.0 and $\hat{k}$=7.0, respectively. (For interpretation of the references to colour in this figure legend, the reader is referred to the web version of this article.)

regimes, to its right and top - catastrophic sliding, and to its left and bottom - arrested sliding.

It is first observed that if both $\hat{p}_{init} < p^*$ and $\hat{v}_{init} < v^*$, the initial conditions lie below the separatrix, in domain 3 or 4, and thus the slide will develop as an arrested slide. Here, we wish to consider the more interesting cases where the initial conditions lie in any one of the phase plane domains. For that, we examine two sets of initial conditions, corresponding to the two types of simulations, representing end members of triggering mechanisms: Type *A* with $\hat{p}_{init} > p^*$ and $\hat{v}_{init} = 0$, and Type *B* with $\hat{v}_{init} > v^*$ and $\hat{p}_{init} = 0$. Changes in permeability affect both the location of the fixed point and the slope of the eigenvectors and may thus affect sliding stability. A permeability increase shifts the fixed point to the right and rotates u_2 clockwise, so that an initial condition that originally resides in domains 1 and 2 can move to domains 4 and 3, respectively, i.e. sliding is stabilized by permeability increase. Fig. 3a demonstrates this behavior, where the initial condition of type *A* is marked by a purple 'x'. Taking a permeability of $\hat{k}=5.9$, the corresponding eigenvectors are the solid green lines. Point *A* lies in this case in domain 1 and represents a catastrophic slide that evolves following the dashed green curve. In contrast, when taking permeability $\hat{k}=6.9$, the corresponding eigenvectors are the solid red lines. Point *A* lies in this case in domain 4 and will evolve following the dashed red curve. Sliding starts by acceleration, but then the mass starts decelerating until sliding is arrested. A similar situation occurs for initial condition of type *B* marked by an orange 'x' in Fig. 3b. For the low permeability, point *B* lies in domain 2, and thus results in a catastrophic slide, while for the larger permeability point *B* lies in domain 3 and will evolve following the curves of an arrested slide.

4.1. Sensitivity study

In this section, the sensitivity of the stability of the sliding process to system parameters is investigated. This goal is achieved by examining the relation between various parameters and the value of the critical permeability, $\hat{k}_c$, that was defined numerically in Section (3). First, $\hat{k}_c$ is defined analytically: For any initial conditions of type *A* or *B* and for any set of parameters, there exists a critical permeability, $\hat{k}_c$, (that dictates the location of the fixed point (9) and the slope of the eigenvectors), such that the specific initial conditions will reside exactly on the separatrix u_2. The physical importance of $\hat{k}_c$ can be understood as follows: When the value of $\hat{k}_c$ is determined for specific initial conditions and set of parameters, the actual permeability (estimated or measured), $\hat{k}$, will dictate whether the slide will be arrested ($\hat{k} > \hat{k}_c$) or catastrophic ($\hat{k} < \hat{k}_c$). In order to find the value of $\hat{k}_c$, a geometrical relation is used: $\hat{k}_c$ is the permeability value for which the slope of the line connecting the initial conditions, (v_{init}, p_{init}), and the fixed point, (v^*,p^*), is exactly the slope of the separatrix u_s:

$$\frac{p^* - p_{\text{init}}}{v^* - v_{\text{init}}} - \text{slope}(u_2) = 0 \tag{11}$$

where $\text{slope}(u_2) = \lambda_2/N\mu$, $\lambda_2 = 0.5\left[J_{22} - \sqrt{J_{22}^2 - 4J_{12}J_{21}}\right]$ and J_{ij} is given in Eq. (10). Eq. (11) is an implicit equation for $\hat{k}_c$ as function of v^* and J_{22}. Using parameter values from Table 1, we calculate from Eq. (11) that for point *A*, $\hat{k}_c=6.2$, and for point *B*, $\hat{k}_c=6.6$. Small deviations from the values of $\hat{k}_c$ found in the numerical analysis result from the simplification involved in the linearization of the diffusion term.

When exploring the effect of system parameters on the value of $\hat{k}_c$ from Eq. (11), it is found that decreasing the diffusion length scale, *l*, leads to a smaller $\hat{k}_c$. Physically it occurs because smaller *l* results in faster diffusion, which causes a bias toward the arrested regime, as PP is maintained along the shear zone for shorter duration. Smaller $\hat{k}_c$ balances this bias as it has the opposite effect of maintaining PP along the shear zone for longer time by decreasing the diffusion coefficient. For similar reasons, increasing the friction coefficient, μ, or decreasing the slope angle, δ, causes $\hat{k}_c$ to drop. Increasing the shear zone thickness, *d*, also decreases the value of $\hat{k}_c$ as it causes the heat generated by frictional heating to be spread along thicker shear zone and thus generate less PP by thermal pressurization. In contrast to the above parameters, modification of slide thickness, *D*, has no effect on the system behavior as both the diffusion process controlling PP evolution and the force balance controlling velocity evolution are independent of *D*, as shown in Goren and Aharonov (2007). However, for natural cases, the permeability at the base of thick slides is expected to be smaller than the permeability at the base of thinner slides due to the natural decrease of permeability with depth (Manning and Ingebritsen, 1999; Saar and Manga, 2004). For that reason, thicker slides are potentially more catastrophic than thinner slides, and also have longer runout (Goren and Aharonov, 2007).

5. Creeping motion of landslides

An additional regime of landslide kinematics that is observed in nature is creeping motion (Radbruch-Hall, 1978). An example of such motion is the La Clapière landslide in the French Alps that is characterized by decades of creep, with a velocity that varies by an order of magnitude, between 1–10 mm/day (Cappa et al., 2004; Guglielmi et al., 2005). In this section we present a hypothesis that explains creep motion of landslides as a sequence of many short arrested events. It should be stressed that the validity of our analysis to a single arrested event is independent of this hypothesis.

Table 2 presents a new set of parameters used for solving the model presented in Section 2. The new set includes a steeper slope of $\delta=30°$ corresponding to the average slope of the failure plane of La Clapière (Helmstetter et al., 2004; Cappa et al., 2004; Guglielmi et al., 2005). As it is required that prior to triggering the slope is stable, the angle of internal friction is taken as $\mu=0.6>\tan\delta$. For the same reason, the block is not assumed fluid saturated but rather the water table is taken at dimensionless height $\hat{w}$ above the slide base. Pore pressure prior to sliding onset is then $\hat{p}_0(\hat{z}>\hat{w})=0$ and $\hat{p}_0(\hat{z}\le\hat{w})=\cos\delta\rho_f(\hat{w}-\hat{z})/\rho$. For these parameters, the reference permeability is chosen to be $k_0=10^{-14}$ m^2, corresponding to the order of magnitude for which the transition between the arrested and catastrophic regimes occurs. Fig. 4a shows model results with the new set of parameters (Table 2) for type *A* simulations. Here, the bifurcation occurs after 1 s from sliding onset. An arrested event with $\hat{k}=1.6$ halts after ~5 s, and a traveling distance of $L=0.28$ mm. It is hypothesized that creep motion may be generated by a sequence of many such arrested events. For example, a sequence of 18 such events, assuming the rest of the day the sliding velocity is zero, results in a time averaged velocity of $L\times 18$ events/day = 5 mm/day for that day. Similarly a sequence of 71 such

Table 2
Model parameters used in Section 5

Symbol[a]		Value
Parameters:		
k_0	Reference permeability	10^{-14} m^2
μ	Tangent to the angle of internal friction	0.6[b]
δ	Slope angle	30°[c]
$\hat{w}$	dimensionless height of water table	0.0824
Derived dimensionless variables:		
M	$k_0 d/\eta S\sigma\sqrt{gD}D^2$	1.06×10^{-9}
Σ	$\cos\delta$-$p_0(z=0)$	0.83
M'	MD^2/d^2	0.001
Initial condition:		
$\hat{p}_{init}$	for type *A* simulations	1.42×10^{-4}

[a] Parameters not appearing here are the same as in Table 1.
[b] A relatively large value for the friction coefficient is used so that the slope will be stable without external triggering over the relatively steep slope in the absence of cohesion, which is not taken here into account.
[c] Following the slope angles of La Clapière (Helmstetter et al., 2004).

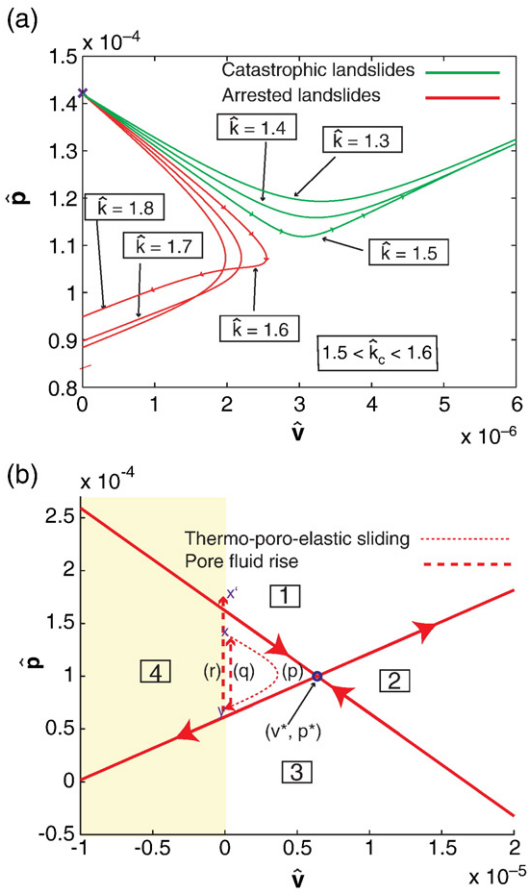

Fig. 4. (a) Numerical simulations with parameters from Table 2. (b) A possible scheme for the generation of creep motion of landslide. Continuous repetition along path (p) representing an arrested thermo-poro-elastic event and path (q) representing pore fluid pressurization may result in creeping motion. If pore fluid is pressurized to higher values along path (r), the landslide will reach the catastrophic regime. Shaded area at the left of the phase plane represents the range of non-physical negative dimensionless velocity.

arrested events results in a time averaged velocity of 20 mm/day. Thus, the averaged daily creep velocity for a specific day is a function of the number of arrested events occurring during that day.

Fig. 4b illustrates a possible scheme for sequencing many arrested events. An arrested event starting from point 'x' follows the thin dashed thermo-poro-elastic path, (p), to point 'y' where it halts. Then, rainfall and snowmelt infiltrate into the shear zone (Pouya et al., 2007), causing pore fluid pressure rise along path (q) back to 'x'. Here, the block is unstable on the slope, and thermo-poro-elastic sliding may occur again along path (p). According to this scheme, the number of daily arrested events depends on the rate of pore fluid infiltration and accumulation within the shear zone. If this rate is high, (for example during heavy and long rain), the number of arrested events will be large and the recorded daily averaged creep velocity will be high, corresponding to the peaks of the creep velocity time series (e.g. Pouya et al., 2007). If this rate is low, then the number of arrested events and the recorded average velocity for that day will be small. This sequencing scheme provides a simple explanation for the daily variations in creep velocity characterizing La Clapière landslide and in particular for deceleration periods (Helmstetter et al., 2004).

A similar mechanism may have operated during the creeping stage of Vaiont landslide that preceded its acceleration. (Although we cannot know for sure, since the fluctuations in the creep velocity were not measured). Helmstetter et al. (2004) describe a series of attempts to fill the dammed reservoir at the foot of the landslide. Each such attempt was followed by increasing creep velocity that was reduced by lowering back the reservoir water level. In 1963 the creeping velocity was not reduced by the same procedure but instead developed into a catastrophic landslide (Radbruch-Hall, 1978). Here again, the controlled creeping may have operated as a sequence of arrested events, following repeatedly the (p)–(q) pass in Fig. 4b. The 1963 reservoir filling might have caused larger pore pressure elevation following path (r) instead of (q) so that the new conditions lie in domain 1 of the phase plane which corresponds to catastrophic regime.

6. Discussion

The analysis presented here shows that thermo-poro-elastic (TPE) feedbacks lead sliding blocks to slide in one of two very distinct kinematics regimes: When the permeability is small, the block's velocity and pore pressure will increase during sliding and thus sliding will accelerate. (Possible examples of this regime are the Vaiont and Val Pola landslides). In contrast, when the permeability is high, the sliding block will first accelerate, then decelerate and rapidly halt. The arrested sliding regime may explain the type of short sliding movement described in Day et al. (1999), Gabet and Mudd (2006) and Bartelt et al. (2007) as it shows relatively short travel distance and self stabilization on the slope over which the sliding was initiated. The sliding distance of an arrested event depends on the physical parameters: Model runs with the parameters given in Table 1 lead to sliding distances of the order of 1 m, while model runs using the parameters given in Table 2, with a lower water table, lead to arrested events that slide less than a mm. It is speculated that a sequence of very short arrested events of the form produced by the parameters of Table 2 may be interpreted as a creeping landslide with average velocity that depends on the number of events in the sequence.

It should be noted that this study focuses on the first few seconds of the sliding process. For that reason, the simplification adopted here, that the permeability is constant with time, has a minor affect on the model results, as the permeability is not expected to vary significantly during the short modeled duration. Catastrophic landslides, which are a possible outcome of our model, will continue and evolve beyond the time scale investigated here. Results from simulations performed over a longer duration (keeping the system parameters constant) are depicted in Fig. 5. For the parameters given in Table 1, excess PP approaches the initial effective normal stress after about 50 s from sliding onset. From that point on frictional resistance becomes minimal and the velocity increases continuously as if the slide will never halt. Temperature at the shear zone increases monotonously and thus will reach values for which the assumption of liquid pore fluid is no longer valid. For natural cases however, a slide that lies initially in the catastrophic regime will eventually halt when its energy is dissipated (Nicoletti and Sorriso-Valvo, 1991) either when the slope becomes less steep and frictional resistance to sliding is increased, or when the sliding block internal parameters, such as the permeability, are changed due to mass fragmentation, as will be discussed below.

In the framework of a TPE model the dependence of sliding stability on permeability is expected. Pore pressure is generated within the shear zone by thermal pressurization caused by frictional heating. A pore pressure increase reduces the effective stress and promotes high sliding velocity. Higher velocities in turn increase the rate of heat generation by friction and thus produce further thermal pressurization. This feedback is countered by pore pressure diffusion from the shear zone. If diffusion rates surpass generation rates, pore pressure within the shear zone will decrease and frictional resistance will arrest the sliding block. If however the rate of diffusion is smaller than the rate of generation by thermal pressurization, pore pressure within the shear zone will rise and sliding velocity will increase. Eq. (4) shows that the diffusion rate depends linearly on the permeability, thus the higher the permeability the more stable the sliding is.

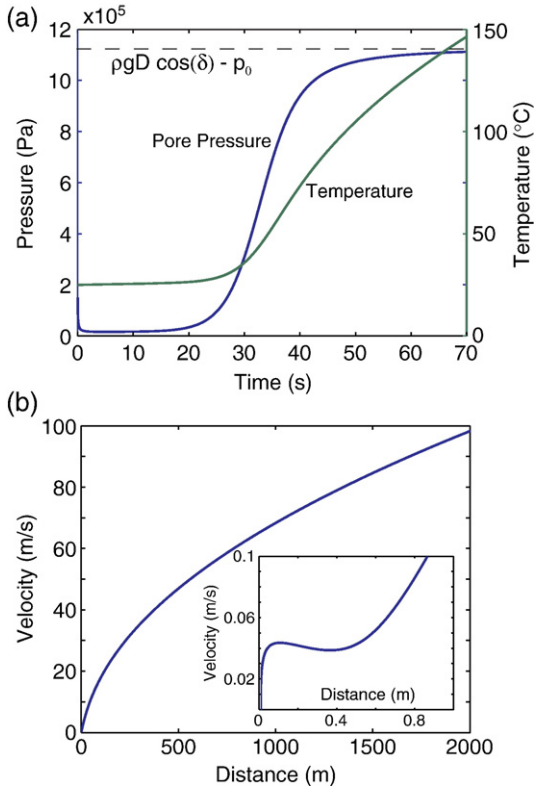

Fig. 5. Extension of simulation for a catastrophic slide with initial condition of type *A* and $\hat{k}=6.9$ for sliding distance of 2000 m. (a) Excess pore pressure and temperature along the shear zone as a function of sliding duration showing that excess PP approaches the value of the initial effective normal stress after about 50 s from slide onset. Temperature increases monotonously due to the slowness of temperature relaxation (see text). (b) Velocity as a function of sliding distance showing a continuous increase after a short episode of decrease that is depicted in the inset. Velocity decrease corresponds to the loop in the velocity PP phase plane depicted in the inset of Fig. 2a.

For any given natural slide, the permeability is expected to vary with sliding distance as sliding motion is expected to cause fracturing, which will lead to a permeability increase. Therefore, a sliding block which starts in the catastrophic regime, might eventually self-stabilize by a dynamic permeability increase. Such a scenario is hypothesized to apply to the Heart Mountain landslide. This 2–4 km thick landslide in north-west Wyoming was initiated along a shallow slope dipping 2°. It accelerated and attained a travel distance of tens of kilometers, stopping on the same low dipping slope (Pierce, 1973). Heart Mountain landslide was suggested to be triggered by pore fluid thermal and mechanical pressurization (Aharonov and Anders, 2006). In the framework of the model presented here, it is speculated that this triggering placed the Heart Mountain landslide in domain 1 of the phase space (Fig. 3), where it started as a catastrophic landslide. The extensive fragmentation it suffered during the sliding process increased its permeability enough to shift it to the arrested regime which allowed it to stop on the same slope over which it was initiated.

"Competition" between driving forces and resisting forces was studied before in the context of landslide mobility. For example, Iverson et al. (2000); Savage and Iverson (2003) and Iverson (2005) studied the interplay between slide acceleration due to pressurization by porosity reduction and the friction increase due to PP dissipation by diffusion. Also Mangeney-Castelnau et al. (2003) studied the balance between pressure gradients and inertial driving forces and frictional resisting forces. Here, we focus on another potentially important feedback, TPE, that in nature is expected to be coupled to the other mechanisms discussed above, and is considered to be crucial for both landslides (Voight and Faust, 1982; Vardoulakis, 2000, 2002; Goren and Aharonov, 2007) and motion along faults (Garagash and Rudnicki, 2003; Rempel and Rice, 2006; Rice, 2006). The use of the TPE model, which is described by a closed form of a relatively simple set of partial differential equations, enables the novel analytical analysis that reveals the source of bifurcation between the different kinematics regimes. This bifurcation is an outcome of the competition between the driving and resisting forces accounted for here.

When considering the TPE mechanism, modification of other system parameters (in addition to permeability) also have a similar effect of introducing a bifurcation between stability regimes. For example, high thermal pressurization coefficient, Λ, is expected to increase the driving forces and lead to unbounded sliding while a small value of Λ is expected to stabilize a slide. Furthermore, the parameters that were considered as part of the analytical sensitivity study (Section 4.1) have also implications to the slide stability. For example, decrease of shear zone thickness, d, causes an increase to the transition permeability, $\hat{k}_c$. When $\hat{k}_c$ rises the range of permeabilities for which $\hat{k} < \hat{k}_c$ is increased and for all these permeabilities sliding is expected to be catastrophic. Thus, thinner shear zones promote catastrophic slides. Moreover, as part of the simplifications adopted in our model, the shear zone porosity is taken as constant. Accounting for porosity change within the shear zone, Iverson (2005) showed that in the framework of a poro-elastic model dilative shear zones cause PP to decrease and thus will tend to stabilize slides, while contractive shear zones will lead to catastrophic landslides.

Verification of the model presented here by field examples can be achieved by comparing model results to natural landslides. This can be done by measuring the relevant parameters and initial conditions that appear in Table 1 in the field, and assigning them to the model. Then, the following comparisons may be performed: (1) The sliding regime of the natural slide can be compared to the sliding regime predicted by the model. It should be noted that for landslides that traveled great distances and were not viewed by people, it is not always clear whether the nature of the sliding process was catastrophic or creeping. (2) If a sliding process was monitored in the field, model results for the evolution of velocity, PP and temperature can be compared to data collected in the field. (3) For arrested events, model results for the travel distance can be compared to the measured distance. Field examination of the hypothesis that creeping sliding motion may be generated by a series of arrested events requires monitoring the velocity of creeping landslides at a resolution of sub-seconds in order to identify the separate arrested events within the sequence.

Applying the model to natural slopes for landslides hazard analysis requires first measuring the mechanical and hydraulic parameters of the materials composing the slope: density, porosity, internal friction coefficient and permeability. Next, a potential shear zone thickness, depth and angle should be estimated. This estimation can be done by examining geometrical parameters of other slides in the area which have similar mechanical and hydraulic characteristics, or by trying to identify potential failure planes by looking for mechanically weak layers or layers that are hydraulically sealed in their base. Then, for an assumed set of initial conditions the model may be used to estimate the stability of the examined potential slide (whether it will develop as catastrophic or arrested). Initial conditions of type *A* should be considered in locations that suffer from periods of anomalously high precipitation, glacial melting and spring discharge rates. In these cases the value of the initial PP can be estimated as the value that will cause slope instability, i.e. $\hat{p}_{init} \geq \Sigma - \sin\delta/\mu$. Initial conditions of type *B* should be considered for slopes in tectonically active areas and on volcanos flanks. In such cases $\hat{v}_{init}$ should be estimated from potential ground velocity. Despite the expected large uncertainty in the value of the measured and estimated parameters and in particular the expected error in the measured permeability, there will be cases for which the slide will lie strictly in one of the regimes, arrested or catastrophic. The term 'lie strictly' may be understood as if the whole space of parameters uncertainty was assigned to the model and the

model always predicts the same regime for that slide. There will be other cases however for which the examined potential slide will not lie strictly in one of the regime as the model results will vary when different values within the uncertainty space are assign to it. Here, a better constraint of parameters is required.

7. Summary and conclusions

The question of landslide stability emerges from field observations indicating that while most of the studied landslides are of catastrophic nature, there are also landslides with self-arrested behavior that halt on the slope. This question is investigated here using a thermo-poro-elastic (TPE) model that couples shear heating, thermal pressurization of pore fluid and pore pressure (PP) diffusion. The model assumes a 1D block slide with deformation concentrated along a thin shear zone at the slide base. The TPE mechanism, while only one of several possible mechanisms operating during slides, has been increasingly acknowledged as a basic feedback mechanism controlling landslides runout (e.g. Voight and Faust, 1982; Davis et al., 1990; Vardoulakis, 2000, 2002; Goren and Aharonov, 2007) and motion along faults (Garagash and Rudnicki, 2003; Rempel and Rice, 2006; Rice, 2006), and therefore is crucial to study.

This work demonstrates numerically the emergence of the two sliding kinematics regimes – catastrophic and arrested – from the TPE model. An innovative analytical study of the TPE mechanism allows deep understanding of the dependence between sliding kinematics and the mechanical and geometrical parameters of the sliding mass. In particular we focus on the role of the shear zone permeability that is documented to vary greatly laterally between different terrains (Saar and Manga, 2004), vertically with depth (Manning and Ingebritsen, 1999; Saar and Manga, 2004), and temporally with sliding distance. Both the numerical and analytical analyses show that low permeabilities lead to catastrophic landslides, while high permeabilities may lead to self stabilized, arrested slides. A sequence of many arrested events is hypothesized to generate a creeping motion.

The small number of parameters involved in the model presented here (Table 1) allows application of the model to natural cases of potential slope failure in order to assess landslide hazard: assigning the parameters of a potential failure plane with relevant initial conditions (as explained in Section 6) into the model allows estimating whether the actual failure will accelerate catastrophically, arrest, or it is still undetermined due to parameter uncertainty.

A similar analysis may be applied to the stability of motion along geological faults: Garagash and Rudnicki (2003) model TPE sliding of faults and show two regimes of stability for fault sliding — arrested and catastrophic. Thus, the new understanding regarding the role of permeability in controlling sliding stability is directly applicable to tectonic faults and to earthquakes.

Acknowledgements

We thank Claude P. Jaupart, Oliver Korup, and Anne Mangeney for very helpful remarks.

References

Aharonov, E., Anders, M.H., 2006. Hot water: A solution to the Heart Mountain detachment problem? Geology 34 (3), 165–168, doi:10.1130/G22027.1.
Aharonov, E., Sparks, D., 2002. Shear profiles and localization in simulations of granular materials. Phys. Rev. E 65, 5.
Bartelt, P., Buser, O., Platzer, K., 2007. Starving avalanches: Frictional mechanisms at the tail of finite-sized mass movements. Geophys. Res. Lett. 34, doi:10.1029/2007GL031352.
Cappa, F., Guglielmi, Y., Soukatchoff, V.M., Mudry, J., Bertrand, C., Charmoille, A., 2004. Hydromechanical modeling of a large moving rock slope inferred from slope levelling coupled to spring long-term hydrochemical monitoring: example of the La Clapière landslide (Southern Alps, France). J. Hydrol. 291, 67–90, doi:10.1016/j.jhydrol.2003.12.013.
Crosta, G., Chen, H., Lee, C., 2004. Replay of the 1987 Val Pola landslide, Italian Alps. Geomorphology 60, 127146, doi:10.1016/j.geomorph.2003.07.015.
Davis, R.O., Smith, N.R., Salt, G., 1990. Pore fluid frictional heating and stability of creeping landslides. Int. J. Num. Anal. Meth. Geomech. 14, 427–443.
Day, S.J., Carracedo, J.C., Guillou, H., Gravestock, P., 1999. Recent structural evolution of the Cumbre Vieja volcano, La Palma, Canary Islands: volcanic rift zone reconfiguration as a precursor to volcano flank instability? J. Volc. Geotherm. Res. 94, 135–167.
Gabet, E.J., Mudd, S.M., 2006. The mobilization of debris flows from shallow landslides. Geomorphology 74, 207–218, doi:10.1016/j.geomorph.2005.08.013.
Garagash, D.I., Rudnicki, J.W., 2003. Shear heating of a fluid-saturated slip weakening dilatant fault zone 1. limiting regimes. J. Geophys. Res. 108, B2 2121, doi:10.1029/2001JB001653.
Genevois, R., Ghirotti, M., 2005. The 1963 Vaiont landslide. G. Geol. Appl. 1, 41–52.
Goren, L., Aharonov, E., 2007. Long runout landslides: The role of frictional heating and hydraulic diffusivity. Geophys. Res. Lett. 34, L07301, doi:10.1029/2006GL028895.
Guglielmi, Y., Cappa, F., Binet, S., 2005. Coupling between hydrogeology and deformation of mountainous rock slopes: Insights from La Clapiµere area (southern Alps, France). C. R. Geosci. 337 (13), 1154–1163, doi:10.1016/j.crte.2005.04.016.
Haneberg, W.C., 1991. Pore pressure diffusion and the hydrologic response of nearly saturated, thin landslide deposits to rainfall. J. Geol. 99 (6), 886–892.
Helmstetter, A., Sornette, D., Grasso, J.R., Andersen, J.V., Gluzman, S., Pisarenko, V., 2004. Slider block friction model for landslides: Application to Vaiont and La Clapiµere landslides. J. Geophys. Res. 109, doi:10.1029/2002JB002160.
Hewitt, K., Clague, J.J., Orwin, J.F., 2008. Legacies of catastrophic rock slope failures in mountain landscapes. Earth-Sci. Rev. 87, 1–38, doi:10.1016/j.earscirev.2007.10.002.
Iverson, R.M., 1997. The physics of debris flows. Rev. Geophys. 35 (5), 245–296.
Iverson, R.M., 2000. Landslide triggering by rain infiltration. Water Resour. Res. 36 (7), 1897–1910.
Iverson, R.M., 2005. Regulation of landslide motion by dilatancy and pore pressure feedback. J. Geophys. Res. 110, doi:10.1029/2004JF000268.
Iverson, R.M., Reid, M.E., Iverson, N.R., LaHusen, R.G., Logan, M., Mann, J.E., Brien, D.L., 2000. Acute sensitivity of landslide rates to initial soil porosity. Science 290 (5491), 513–516, doi:10.1126/science.290.5491.513.
Lourenço, S.D.N., Sassa, K., Fukuoka, H., 2006. Failure process and hydrologic response of a two layer physical model: Implications for rainfall-induced landslides. Geomorphology 73 (1–2), 115–130, doi:10.1016/j.geomorph.2005.06.004.
Mangeney, A., Tsimring, L.S., Volfson, D., Aranson, I.S., Bouchut, F., 2007. Avalanche mobility induced by the presence of an erodible bed and associated entrainment. Geophys. Res. Lett. 34, L22401, doi:10.1029/2007GL031348.
Mangeney–Castelnau, A., Vilotte, J. –P., Bristeau, M.O., Perthame, B., Bouchut, F., Simeoni, C., Yerneni, S., 2003. Numerical modeling of avalanches based on saint venant equations using a kinetic scheme. J. Geophys. Res. 108 (B11), doi:10.1029/2002JB002024, 2003.
Manning, C.E., Ingebritsen, S.E., 1999. Permeability of the continental crust: Implications of geothermal data and metamorphic systems. Rev. Geophys. 37 (1), 127–150.
Nicoletti, P.G., Sorriso-Valvo, M., 1991. Geomorphic controls of the shape and mobility of rock avalanches. GSA Bulletin 103 (10), 1365–1373.
Pierce, W.G., 1973. Principle features of the Heart Mountain fault and the mechanism problem. In: Scholten, R., D. J., K.A. (Eds.), Gravity and Tectonics. John Wiley and Sons, New York, pp. 457–471.
Pouya, A., Léonard, C., Alfonsi, P., 2007. Modelling a viscous rock joint activated by rainfall: Application to the La Clapiµere landslide. Int. J. Rock Mech. Min. Sci. 44, 120–129, doi:10.1061/j.ijrmms.2006.05.004.
Radbruch-Hall, D., 1978. Gravitational creep of rock masses on slopes. In: Voight, B. (Ed.), Rockslides and Avalanches. . Natural Phenomena. Elsevier, Amsterdam, pp. 607–657. Ch. 17.
Rahardjo, H., Ong, T.H., Rezaur, R.B., Leong, C., 2007. Factors controlling instability of homogeneous soil slopes under rainfall. J. Geotech. Geoenviron. Eng. 133, 1523–1543, doi:10.1061/(ASCE)1090-0241(2007)133:12(1532).
Reid, M.E., 1997. Slope instability caused by small variations in hydraulic condectivity. J. Geotech. Environ. Eng. 123 (8), 717–725.
Rempel, A.W., Rice, J.R., 2006. Thermal pressurization and onset of melting in fault zone. J. Geophys. Res. 111, B09314, doi:10.1029/2006JB004314.
Rice, J.R., 2006. Heating and weakening of faults during earthquake slip. J. Geophys. Res. 111, B05311, doi:10.1029/2005JB004006.
Saar, M.O., Manga, M., 2004. Depth dependence of permeability in the Oregon Cascades inferred from hydrogeologic, thermal, seismic and magnetic modeling constraints. J. Geophys. Res. 109, B04204, doi:10.1029/2003JB002855.
Savage, S.B., Iverson, R.M., 2003. Surge dynamics coupled to pore-pressure evolution in debris flows. In: Chen, R. (Ed.), In Debris-Flow Hazards Mitigation: Mechanics, Prediction and Assessment. Millepress, Rotterdam, pp. 503–514.
Sidle, R.C., Ochiai, H., 2006. Landslides processes, Prediction, and Land Use. American Geophysical Union, Washington, DC.
Strogatz, S.H., 2000. Nonlinear dynamics and chaos. Perseus Publishing, Cambridge, Massachusetts.
Turrini, M.C., Visintainer, P., 1998. Proposal of a method to define areas of landslide hazard and application to an area of the Dolomites, Italy. Engineering Geology 50 (3–4), 255–265.
Vardoulakis, I., 2000. Catastrophic landslides due to frictional heating of the failure plane. Mech. Coh. Frict. Mat. 5, 443–467.
Vardoulakis, I., 2002. Dynamic thermo-poro-mechanical analysis of catastrophic landslides. Géotechnique 52 (3), 157–171.
Voight, B., Faust, C., 1982. Frictional heat and strength loss in some rapid landslides. Géotechnique 32 (1), 43–54.
Ward, S.N., Day, S., 2001. Cumbre Vieja Volcano — potential collapse and tsunami at La Palma, Canary Island. Geophys. Res. Lett. 28 (17), 3397–3400.